JOURNAL OF GUIDANCE, CONTROL, AND DYNAMICS
Vol. 37, No. 1, January–February 2014

Implementation of a Flapping Wing Micro Air Vehicle Control Technique

Michael L. Anderson*
U.S. Air Force Research Laboratory, Eglin Air Force Base, Florida 32578
and
Richard G. Cobb†
Air Force Institute of Technology, Wright–Patterson Air Force Base, Ohio 45433

DOI: 10.2514/1.57855

Flapping wing micro air vehicles continue to be a growing field, with ongoing research into unsteady, low Reynolds number aerodynamics, microfabrication, and fluid–structure interaction. However, research into flapping wing control of such micro air vehicles continues to lag. Existing research uniformly consists of proposed control laws that are validated by computer simulations of quasi-steady blade-element formulas. Such simulations use numerous assumptions and cannot be trusted to fully describe the flow physics. Instead, such control laws must be validated on hardware. In earlier work, a novel control technique, biharmonic amplitude and bias modulation, was proposed and analyzed with these same quasi-steady blade-element formulas. In this work, the biharmonic amplitude and bias modulation control technique was implemented on a flapping wing prototype (4 cm wing length) and tested on a six-component force/torque sensor. Experiments verified that the prototype can generate nearly uncoupled forces and moments for motion in five degrees of freedom when using the biharmonic amplitude and bias modulation control technique, and that these forces can be reasonably predicted by the blade-element formulas.

Nomenclature

A	=	stroke amplitude, rad
C_L	=	lift coefficient
C_D	=	drag coefficient
$D_{(R/L)U}$	=	instantaneous drag during upstroke, N; the R/L subscript, if present, denotes right or left wing
$D_{(R/L)D}$	=	instantaneous drag during downstroke, N; the R/L subscript, if present, denotes right or left wing
$\mathbf{F}_{R/L}^{R/LWS}$	=	instantaneous aerodynamic force from the right (left) wing in the right (left) wing spar frame
I_A	=	second moment of area, m^4
J_n	=	Bessel function of the nth kind
k_L	=	blade element coefficient for lift terms
k_D	=	blade element coefficient for drag terms
L_n	=	nth mechanism link
$L_{(R/L)U}$	=	instantaneous lift during upstroke, N; the R/L subscript, if present, denotes right or left wing
$L_{(R/L)D}$	=	instantaneous lift during downstroke, N; the R/L subscript, if present, denotes right or left wing
M_n	=	nth harmonic coefficient
M_x	=	roll moment, Nmm
M_y	=	pitch moment, Nmm
M_z	=	yaw moment, Nmm
$\mathbf{r}_{\mathrm{cp},R(L)}^{B}$	=	location of the center of pressure of the right (left) wing with respect to the vehicle center of mass
T	=	wing-beat period, s
t	=	time, s
w	=	width, m
X	=	force in the body-fixed x direction, N
x_B	=	micro air vehicle body-fixed x axis
x_{cp}	=	center of pressure location along x axis of the wing, m
Y	=	force in the body-fixed y direction, N
y_B	=	micro air vehicle body-fixed y axis
y_{cp}	=	center of pressure location along y axis of the wing, m
Z	=	force in the body-fixed z direction, N
z_B	=	micro air vehicle body-fixed z axis
α	=	angle of attack, rad
β	=	harmonic phase shift
Δ	=	frequency normalized split cycle parameter
Δx	=	x-axis distance from vehicle center of mass to wing root, m
Δz	=	z-axis distance from vehicle center of mass to wing root, m
η	=	wing stroke bias angle, rad
θ	=	elevation angle, rad
θ_n	=	rotation angle of the nth link, rad
ρ	=	air density, kg/m^3
τ	=	stroke reversal time shift, s
ϕ	=	wing stroke angle, rad
$\dot{\phi}$	=	wing angular velocity, rad/s
ω	=	flapping frequency, rad/s

I. Introduction

RESEARCH into insect-sized flapping wing flight is ongoing, and several prototypes have been developed, with some capable of lifting off the ground in uncontrolled, tethered experiments [1,2]. Although larger, bird-sized flapping wing micro air vehicles (FWMAVs) have flown freely, they are typically controlled by a tail with traditional control surfaces. Such techniques are expected to become ineffective as vehicle size and speed are reduced because of the reduced efficiency of airfoils at low *Re*. Instead, just like insects, the flapping wings themselves will need to be used to generate the necessary forces and moments to control the vehicle. This can be accomplished by altering the wing flapping trajectory or kinematics in precise ways to carefully modulate the forces and moments acting on the vehicle.

Figure 1 is a proposed hierarchal breakdown for insect-sized flapping wing control of a micro air vehicle (MAV). This work focuses on the shaded region of the figure; a controller that achieves a desired vehicle attitude by enforcing the appropriate wing kinematics [3,4]. This is a two-step process. First, given a desired vehicle attitude (translational and rotational velocities), the vehicle motion controller determines the wing kinematics necessary based on the control law.

Received 7 February 2012; revision received 3 March 2013; accepted for publication 18 April 2013; published online 27 December 2013.

*Micro Air Vehicle Program Manager, 101 W. Eglin Blvd. Senior Member AIAA.

†Associate Professor, Department of Aeronautics and Astronautics, 2950 Hobson Way. Associate Fellow AIAA.

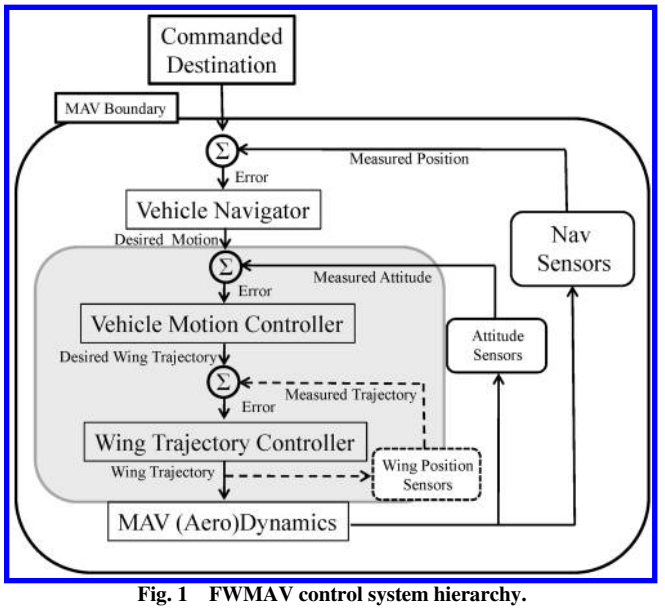

Fig. 1 FWMAV control system hierarchy.

Second, this desired wing motion is created by the wing flapping actuators under the direction of the wing trajectory controller, preferably without the need to measure and feedback wing position (which would reduce weight and complexity). The crux of this process is developing the control law; how should the wings be flapped to create the desired vehicle motion?

Several such control laws have been proposed for flapping wing MAVs and validated to various degrees through simulation [5–15]. In previous work, a novel FWMAV control technique was proposed called biharmonic amplitude and bias modulation (BABM) [15]. It requires a vehicle capable of arbitrarily and independently prescribing the position of each wing as a function of time, with the corresponding benefit that the vehicle only needs to be capable of actively controlling one degree of freedom (DOF) per wing, as compared with insects that actively control three DOF per wing. Consider Fig. 2, which defines the wing kinematics and body-fixed coordinate frame.

Three angles define the position and orientation of the wing at any point in time; stroke angle ϕ, elevation angle θ, and angle of attack α. For BABM control, elevation angle is held fixed, and angle of attack is controlled by a passive wing rotation joint and assumed to be constant for the derivation. Therefore, only the stroke angle is prescribed. The stroke angle function is deliberately constructed with three control parameters (variables that can be adjusted in flight) that will directly influence DOFs of the MAV, and thus provide a means for attitude control. This stroke angle function could be applied symmetrically to both wings, or asymmetrically to obtain the desired control effect. Ideally, this stroke angle function would be able to influence all six of the MAV DOFs, and there would be little coupling between DOFs. This influence will be determined below for the wing stroke angle function

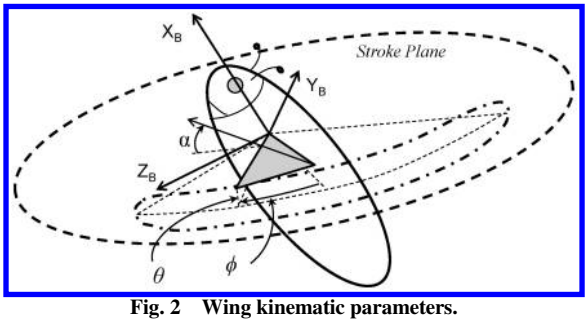

Fig. 2 Wing kinematic parameters.

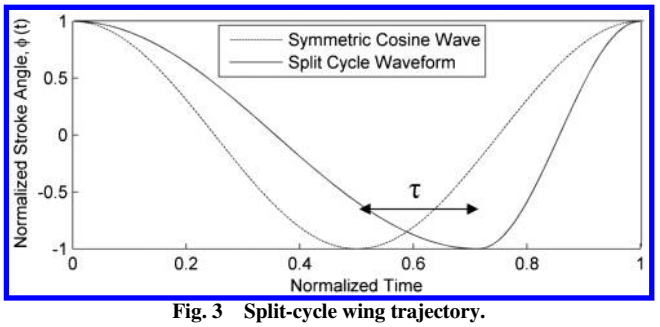

Fig. 3 Split-cycle wing trajectory.

$$\phi(t) = A\{M_1(\tau)\cos[\omega t + \beta(\tau)] - M_2(\tau)\sin[2\omega t + 2\beta(\tau)]\} + \eta \tag{1}$$

where the three control parameters A, η, and τ are stroke amplitude, stroke bias, and stroke reversal time shift, respectively, and M_1, M_2, and β are harmonic coefficients and phase shifts that are functions of τ defined as

$$M_1(\tau) = \cos(2\tau) \tag{2}$$

$$M_2(\tau) = 0.34\,\sin(3.3\tau) \tag{3}$$

$$\beta(\tau) = -2\tau \tag{4}$$

These harmonic amplitude coefficient and phase shift functions were carefully selected as the result of a Fourier sum analysis to create a split-cycle waveform, which is a wing trajectory whose upstrokes and downstrokes are not symmetric, as would be the case for simple harmonic motion where the reversal from downstroke to upstroke occurs at half the stroke period [3]. With the split cycle waveform, the reversal is time-shifted by approximately $\pm\tau$, as shown in Fig. 3. This asymmetric waveform will create a net nonzero drag on the MAV when averaged over a wing-beat period, a force which can then be used as an input for vehicle control. The waveform is constructed as a sum of two harmonic terms because this creates a continuous function without introducing high frequency terms. High frequency content in the wing trajectory will be filtered out by the wing flapping mechanism, and so such a desired wing trajectory would not be feasible for an insect-sized MAV wing [3,4]. Furthermore, if the wings will be driven at the resonant frequency of the system, which is desirable for energy efficiency, this filtering will be significant and will complicate the implementation of any nonharmonic wing trajectory.

Given this proposed BABM wing trajectory, it is desirable to predict how perturbations to it influence the motion of the vehicle. This can be accomplished using a process developed by Doman and Oppenheimer [7] and Doman et al. [8]. This consists of making blade-element estimates of the instantaneous lift and drag forces on each wing in a local wing reference frame, transforming those forces into a body-fixed frame to obtain instantaneous forces and moments, integrating these over a wing-beat period to obtain cycle-averaged forces and moments, and finally, taking partial derivatives of these cycle-averaged values with respect to each control parameter to obtain linearized control derivatives. These control derivatives indicate how each variable feature of the wing trajectory influences the MAV motion. This process was described in detail for the BABM trajectory in previous work, and so it will only be reviewed here [15].

The magnitudes of the wing's instantaneous lift and drag forces in a local wing reference frame are [7]

$$L = k_L\dot{\phi}^2 \tag{5}$$

$$D = -k_D\dot{\phi}|\dot{\phi}| \tag{6}$$

$$k_D = \frac{\rho}{2} C_D I_A \qquad k_L = \frac{\rho}{2} C_L I_A \tag{7}$$

These wing forces impart time-varying forces and moments on the MAV body. The resulting body forces are obtained through coordinate transformations that depend on the time-varying wing stroke angle:

$$X_R^B = k_L \dot{\phi}_R^2 \tag{8}$$

$$X_L^B = k_L \dot{\phi}_L^2 \tag{9}$$

$$Y_R^B = k_D \dot{\phi}_R |\dot{\phi}_R| \sin \phi_R \tag{10}$$

$$Y_L^B = -k_D \dot{\phi}_L |\dot{\phi}_L| \sin \phi_L \tag{11}$$

$$Z_R^B = -k_D \dot{\phi}_R |\dot{\phi}_R| \cos \phi_R \tag{12}$$

where

$$Z_L^B = -k_D \dot{\phi}_L |\dot{\phi}_L| \cos \phi_L \tag{13}$$

The body moments depend on the time-varying location of the center of pressure of each wing according to the cross product $\mathbf{M}^B = \mathbf{r}_{\text{cp}}^B \times \mathbf{F}^B$. They are

$$M_{XR}^B = -k_D \dot{\phi}_R |\dot{\phi}_R| \left[y_{\text{CP}} + \frac{w}{2} \cos \phi_R + \Delta z \sin \phi_R \right] \tag{14}$$

$$M_{XL}^B = k_D \dot{\phi}_L |\dot{\phi}_L| \left[y_{\text{CP}} + \frac{w}{2} \cos \phi_L + \Delta z \sin \phi_L \right] \tag{15}$$

$$M_{YR}^B = k_L \dot{\phi}_R^2 [\text{sgn}(\dot{\phi}_R) x_{\text{cp}} \cos \phi_R \cos \alpha + y_{\text{cp}} \sin \phi_R + \Delta z] + k_D \dot{\phi}_R |\dot{\phi}_R| [x_{\text{cp}} \cos \phi_R \sin \alpha + \Delta x \cos \phi_R] \tag{16}$$

$$M_{YL}^B = k_L \dot{\phi}_L^2 [\text{sgn}(\dot{\phi}_L) x_{\text{cp}} \cos \phi_L \cos \alpha + y_{\text{cp}} \sin \phi_L + \Delta z] + k_D \dot{\phi}_L |\dot{\phi}_L| [x_{\text{cp}} \cos \phi_L \sin \alpha + \Delta x \cos \phi_L] \tag{17}$$

$$M_{ZR}^B = k_L \dot{\phi}_R^2 \left[\text{sgn}(\dot{\phi}_R) x_{\text{cp}} \sin \phi_R \cos \alpha - y_{\text{cp}} \cos \phi_R - \frac{w}{2} \right] + k_D \dot{\phi}_R |\dot{\phi}_R| [x_{\text{cp}} \sin \phi_R \sin \alpha + \Delta x \sin \phi_R] \tag{18}$$

$$M_{ZL}^B = -k_L \dot{\phi}_L^2 \left[\text{sgn}(\dot{\phi}_L) x_{\text{cp}} \sin \phi_L \cos \alpha - y_{\text{cp}} \cos \phi_L - \frac{w}{2} \right] - k_D \dot{\phi}_L |\dot{\phi}_L| [x_{\text{cp}} \sin \phi_L \sin \alpha + \Delta x \sin \phi_L] \tag{19}$$

These instantaneous body forces and moments are then integrated with respect to time over an entire wing-beat period to obtain cycle-averaged body forces and moments. For example, the cycle-averaged X-body force is

$$\bar{X}_R^B = \frac{\omega}{2\pi} \int_0^T L_R(t)\, \mathrm{d}t = \frac{\omega}{2\pi} \int_0^T k_L \dot{\phi}_R^2\, \mathrm{d}t \tag{20}$$

The resulting 12 cycle-averaged forces and moments describe how the BABM trajectory of each wing influences the entire attitude of the MAV. To predict how the control parameters influence each DOF of the MAV, partial derivatives of each cycle-averaged force or moment are taken with respect to each control parameter to obtain 30 control derivatives that make up the control effectiveness matrix given next. Note that the wing stroke bias modulation η for the two wings is done in unison so that $\eta_R = \eta_L$ and, thus, only five control parameters are available:

$$\begin{bmatrix} \bar{X}^B \\ \bar{Y}^B \\ \bar{Z}^B \\ \bar{M}_X^B \\ \bar{M}_Y^B \\ \bar{M}_Z^B \end{bmatrix} = \omega^2 A_0 \begin{bmatrix} k_L & k_L & 0 & 0 & 0 \\ 0 & 0 & 0 & 0 & 0 \\ 0 & 0 & -k_D J_1(A_0) & -k_D J_1(A_0) & 0 \\ 0 & 0 & -\frac{k_D}{2}\{A_0 y_{\text{cp}} + w J_1(A_0)\} & \frac{k_D}{2}\{A_0 y_{\text{cp}} + w J_1(A_0)\} & 0 \\ 0 & 0 & B_{53} & B_{54} & 2k_L y_{\text{cp}} J_1(A_0) \\ B_{61} & B_{62} & 0 & 0 & 0 \end{bmatrix} \begin{bmatrix} \Delta A_R \\ \Delta A_L \\ \Delta_R \\ \Delta_L \\ \eta \end{bmatrix} \tag{21}$$

where

$$B_{53} = B_{54} = J_1(A_0)\{k_D(\Delta x + x_{\text{cp}} \sin \alpha) + k_L x_{\text{cp}} \cos \alpha\} \tag{22}$$

$$B_{61} = -B_{62} = -k_L \left\{ \frac{w}{2} + \frac{y_{\text{cp}}}{A_0} J_1(A_0) + \frac{y_{\text{cp}}}{2} (J_0(A_0) - J_2(A_0)) \right\} \tag{23}$$

R and L indicate kinematic parameters for the right and left wings, and Δ is the split cycle parameter, a function of the stroke reversal time shift τ defined by

$$\Delta = \frac{2\tau}{1 + 2\tau} \tag{24}$$

These are linearized control derivatives evaluated at the hover condition; ($A = A_0$, $\Delta = 0$, and $\eta = 0$). From the matrix, it is clear how each kinematic parameter imparts a force or moment on the vehicle that can be used to directly control its attitude. Modulating the stroke amplitude has the ability to regulate the vertical force $\bar{X}^B$ and yawing moment $\bar{M}_Z^B$ (see Fig. 4). Modulating the stroke bias can regulate the pitching moment $\bar{M}_Y^B$ whereas modulating the split cycle parameter can regulate horizontal force $\bar{Z}^B$ and rolling moment $\bar{M}_X^B$.

As noted earlier, in addition to the BABM control technique described here, numerous other techniques have been proposed for flapping wing control of MAVs. However, none have been validated on hardware, only tested in simulations that use the same assumptions to test the controls as were used in developing them. Such simulations are an important first step toward demonstrating the feasibility of a control technique, but they do not guarantee it because they use quasi-steady blade-element formulas with numerous

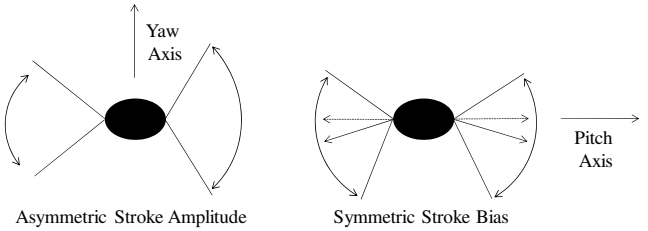

Fig. 4 Wing kinematic parameters A and η used for MAV control.

simplifying assumptions to calculate the aerodynamic forces generated by the wings. Flapping wing flight is highly unsteady due to the periodic wing motion, and no blade-element model exists that can completely capture these effects. Therefore, it is possible that a control technique that is successful in a quasi-steady simulated environment may not be when the full physics are included. To definitively evaluate a proposed control technique, it is necessary to test it in the presence of unsteady effects, not assumption-dependent simulations. This was the major goal of this work.

Given the high computational cost of computational fluid dynamics methods and the quantity of cases that would require testing, the only viable approach to capturing the full aerodynamics is to perform experiments in air. Unfortunately, power and sensing technology are currently insufficient to allow fully autonomous free flight of an insect-sized FWMAV, even if we knew how to control it. However, using a six-component load cell, it is possible to include the complete flow physics while measuring the forces generated by a prototype flapping its wings according to the specified kinematics [16]. It would then be possible to determine if the resulting forces and moments were sufficient to control the vehicle, and the MAV's flight could even be simulated in a hardware-in-the-loop experiment. This would provide an essential intermediate testing step between the current simulations and free flight because it eliminates the most tenuous assumptions of previous FWMAV simulations, replacing them with hardware. Thus, the major contribution of this work was to solve numerous critical hardware implementation issues and perform the most realistic evaluation to date of a flapping wing control technique and its associated assumptions.

II. Wing Trajectory Control

This work will proceed to demonstrate on hardware the feasibility of a flapping wing control technique, BABM. This technique, as well as two other control techniques in the literature, those of Deng et al. [5,6], Doman and Oppenheimer [7], and Doman et al. [8], propose using nonharmonic wing flapping trajectories rather than additional DOF of the wings in order to achieve controllability. Therefore, it is necessary to ensure that the wings track the desired nonharmonic trajectory. In addition, this wing trajectory tracking should be applicable to the resonant flapping frequency of the wing actuation system to provide the maximum energy efficiency for the vehicle. Clearly, at frequencies well below resonance, the wings should track the input well. However, without some compensation, as the drive frequency approaches resonance, one would expect the wing to flap in a harmonic motion, or possibly excite higher modes of the structure as a result of the high frequency content in the split-cycle waveform.

To better understand the wing flapping behavior, a frequency response function (FRF) was measured for the wing flapping system (see Sec. III:) by a laser vibrometer. Note that it is the response of the wing flapping system taken as a whole that is important, not the individual responses of the components: the actuator, wing, etc., will have different frequency responses from the complete system. This system response is shown in Fig. 5. The data were collected by Signal Calc, which is a virtual signal analyzer on a PC. The FRF has a standard underdamped response. The first mode is significant, and so flapping at this frequency would yield a large displacement relative to the energy expenditure, and this mode will be evident in any response because any excitation at that frequency is amplified by at least an order of magnitude.

The desired wing trajectory will be filtered according to these dynamics, and so if they are known in advance, they can be compensated for at each harmonic frequency. The desired BABM trajectory has two harmonics, and so the dynamic response of the wing flapping mechanism at those frequencies is captured by the four terms $M_{\omega 1}$, $M_{\omega 2}$, $\beta_{\omega 1}$, and $\beta_{\omega 2}$, as indicated on the figure. Therefore, an open-loop, feed-forward control is proposed called Discrete Harmonic Plant Compensation (DHPC). With DHPC, the desired BABM trajectory can then be preconditioned to account for these dynamics before feeding it to the actuator by adjusting the harmonic magnitude and phase terms in Eq. (1) as

$$M_{n,\mathrm{PC}} = \frac{M_n}{M_{\omega n}} \quad \text{and} \quad \beta_{n,\mathrm{PC}} = \beta_n - \beta_{\omega n}$$

where $M_{n,\mathrm{PC}}$ and $\beta_{n,\mathrm{PC}}$ are the preconditioned terms. Future insect-sized MAVs are expected to have very little memory and computing power, and so this technique provides a more efficient compensation than a traditional plant inversion technique because only the frequencies of interest are compensated.

The efficacy of this compensation can be seen in Fig. 6 in which the trajectory of a wing flapping mechanism is measured with a laser vibrometer. The results are arranged in three columns corresponding to the percentage of maximum flapping amplitude, then in rows according to the applied split-cycle parameter Δ. The DHPC compensated wing-flapping actuator input voltage is given above each of the measured responses. The desired biharmonic trajectory (dashed) is overlaid on the laser-measured response (solid). Note that the motion of the wing spar is measured at a point 4 mm from the wing root, and the wing is assumed to be a rigid body, an assumption that will be validated by the following experiments. The missing plot corresponding to an amplitude of 100% and a split cycle parameter of 0.25 was not tested because the compensated input voltage would exceed the voltage limits of the actuator.

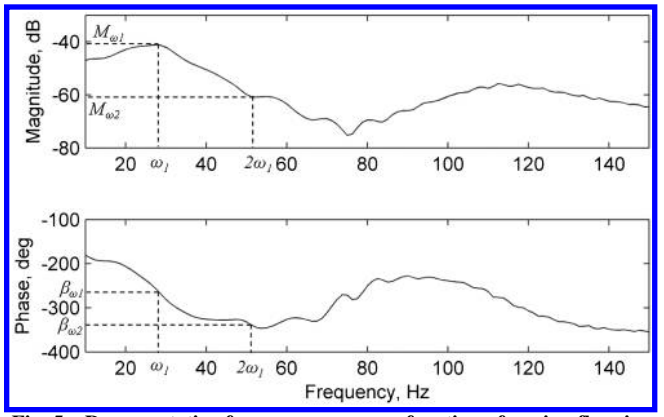

Fig. 5 Representative frequency response function of a wing flapping mechanism.

III. MAV Prototype

The BABM control technique requires a vehicle with the ability to arbitrarily and independently prescribe the stroke angle function of each wing so that the three control parameters can be modulated. Most FWMAV prototypes flap the wings with a DC motor, which enforces nearly simple harmonic wing motion with fixed amplitude and bias. Instead, the vehicle used here uses bimorph cantilever piezo actuators to drive the wings, which have the ability to create more elaborate wing trajectories, including the ability to modulate amplitude and bias and flap nonharmonically with adequate compensation (as described earlier). A detailed description of the design and fabrication of the vehicle is provided in previous work [17], but its design will be summarized here.

A simplified model of the insect flight apparatus is given in Fig. 7. The mechanism can be likened to a simple crank-slider linkage. This, in turn, can be simplified by replacing the slider with a fourth link to create a simple four-bar mechanism; most rotary actuator driven MAVs use a variation on this latter arrangement.

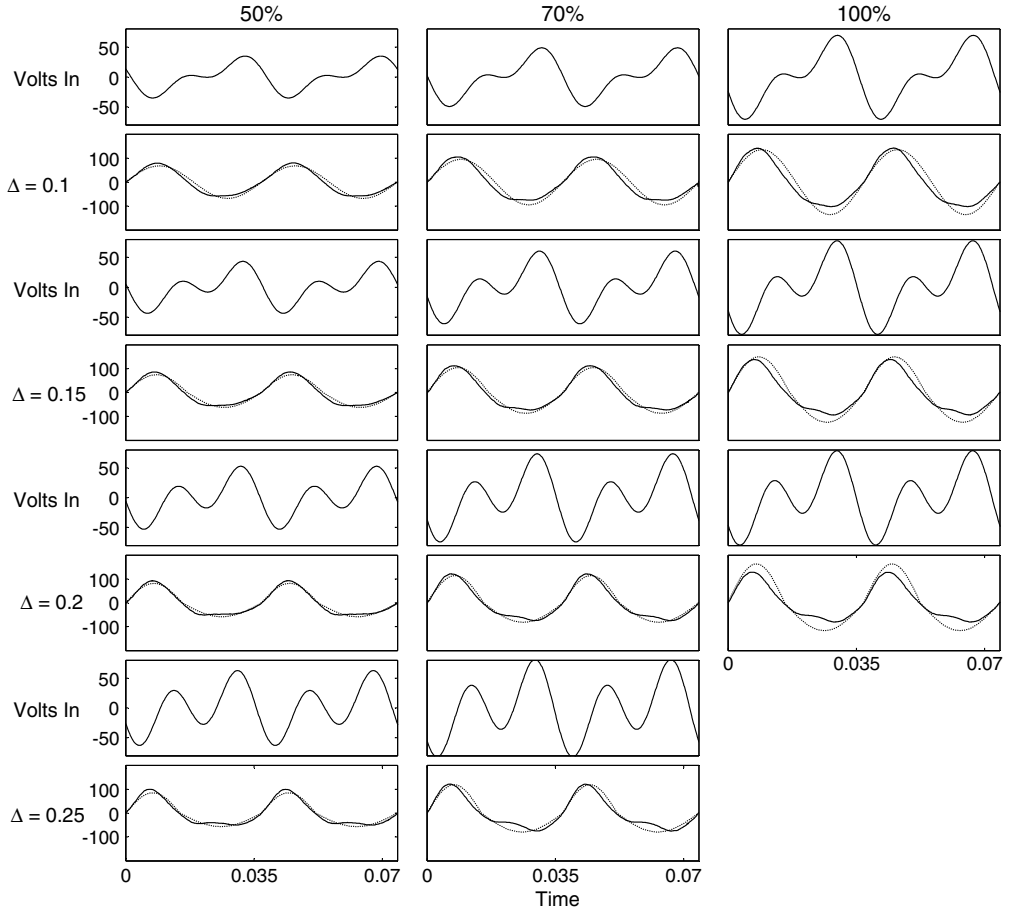

Fig. 6 Wing response to the biharmonic waveform with DHPC.

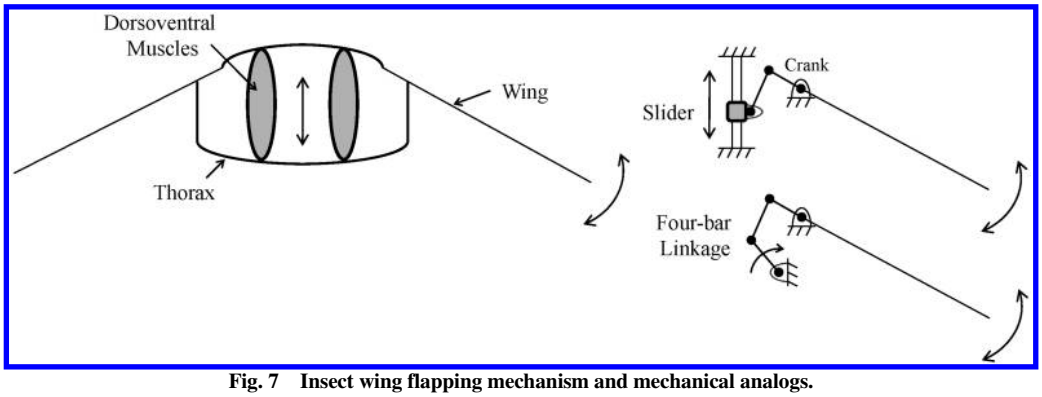

Fig. 7 Insect wing flapping mechanism and mechanical analogs.

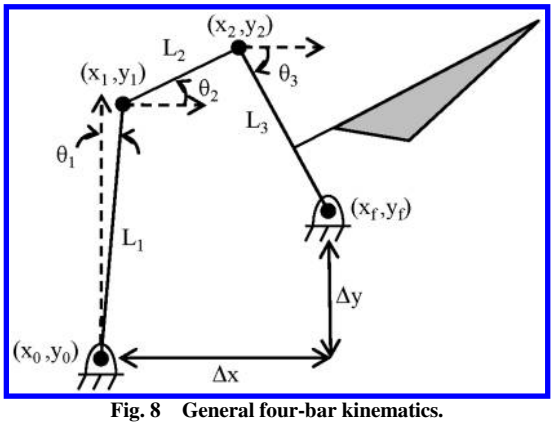

Fig. 8 General four-bar kinematics.

A PZT bimorph cantilever actuator can replace the driving link in the four-bar linkage, creating a simple wing flapping mechanism with the ability to generate arbitrary wing stroke trajectories. The geometry of the linkage and the resulting kinematics are chosen based on the expected displacement of the drive actuator and the desired wing motion. The mechanism was designed to have a maximum wing stroke amplitude of ±55 deg. The actuators are custom made, and designed to have a stroke of ±1 mm.

To design the linkage geometry, a script was created to calculate the linkage kinematics from a given geometry, animate the wing trajectory, and report the maximum and minimum wing stroke angle. The actuator was treated as a rigid body rotating link rather than a flexed cantilever. Figure 8 shows a generic four bar linkage with arbitrary geometry.

Given the prescribed actuator deflection angle θ_1, which is assumed to be small, the location of point (x_1, y_1) can be calculated. It can be shown that

Table 1 Final linkage geometry

Link	Length, mm	Ground position location	
$L1$	30	Δx	1.85
$L2$	2	Δy	28.9
$L3$	1.11		

$$\theta_3 = -\left|2\tan^{-1}\sqrt{\frac{(L_2+L_3)^2-(x^2+y^2)}{(x^2+y^2)-(L_2-L_3)^2}}\right|$$

where $(x, y) = (x_f, y_f) - (x_1, y_1)$ and

$$\theta_2 = \text{atan}\,2(y, x) + \text{atan}\,2(L_3 \sin\theta_3, L_2 + L_3\cos\theta_3)$$

The wing stroke angle is that of θ_3 plus the bias applied by its mounting position on link 3 (90 deg in the figure). The geometry was thus iterated until satisfactory kinematics were achieved. The final design is summarized in Table 1.

The linkage is constructed from 200-μm-thick carbon fiber connected by 12.5 μm Kapton flexures. The wings are 40 mm long with a max chord of 13 mm, and consist of a 2.5-μm-thick Mylar membrane stretched over rigid carbon fiber veins. The wings are attached to the linkage with a flexure joint that allows the wings to rotate passively in response to dynamic pressure until they hit a joint stop, thus enforcing a constant 45 deg angle of attack. Two flapping mechanisms are assembled in a fuselage/test stand in a mirror-image arrangement so that symmetric and asymmetric wing stroke kinematics can be tested. The completed prototype is shown in Fig. 9. This prototype was improved over the previous design iterations by reducing wing inertia to allow for higher flapping frequencies, the addition of wing rotation stops to enforce the angle of attack, and rotating the actuators out of the stroke plane.

IV. Control Force and Moment Measurement

Recall that the purpose of the experiment is to measure the forces and moments generated by the wings when flapped according to the BABM trajectory using DHPC, and thus validate the control effectiveness matrix given in Eq. (21); specifically, to verify that the control parameters influence the DOFs they are predicted to influence, and that coupling between them is limited. Thus, the experiment is to flap the MAV with varying wing trajectories corresponding to the desired range of control parameters while measuring the resultant forces and moments. The wing kinematic/control parameter combinations tested are symmetric amplitude modulation, asymmetric amplitude modulation, symmetric split cycle, and asymmetric split cycle. Wing stroke bias was tested in a tethered motion experiment described next.

Figure 9 showed the MAV prototype and its arrangement on the force/torque sensor, an ATI Nano-17, which has a noise floor on the order of 0.2 mN when unloaded, and is the most sensitive 6-DOF transducer available. Data were captured by an ATI Netbox and imported into a PC for postprocessing. The control parameters are specified to the MAV through a MATLAB Simulink model that constructs the BABM wing trajectory with DHPC for each wing and applies the appropriate actuator voltages through a dSPACE system.

To improve the data, each parameter was tested one at a time with a tare performed between each test point. The upper plot of Fig. 10 shows the test profile for the asymmetric split-cycle test with data taken at seven test points. At each point, the flapping is ramped up to the desired amplitude from zero, data are taken after a pause to allow transients to settle, then the flapping is ramped back down to zero and another tare is taken before the next test. The lower plot is a typical force measurement before postprocessing, showing the correlation with the input.

Figure 11 shows a typical high temporal resolution data capture of the time-varying lift. This profile is consistent with the literature and blade-element predictions indicating lift peaks near mid-stroke and negative lift spikes during wing reversal. For postprocessing, the time-varying force and moment data were averaged over an 8 s period

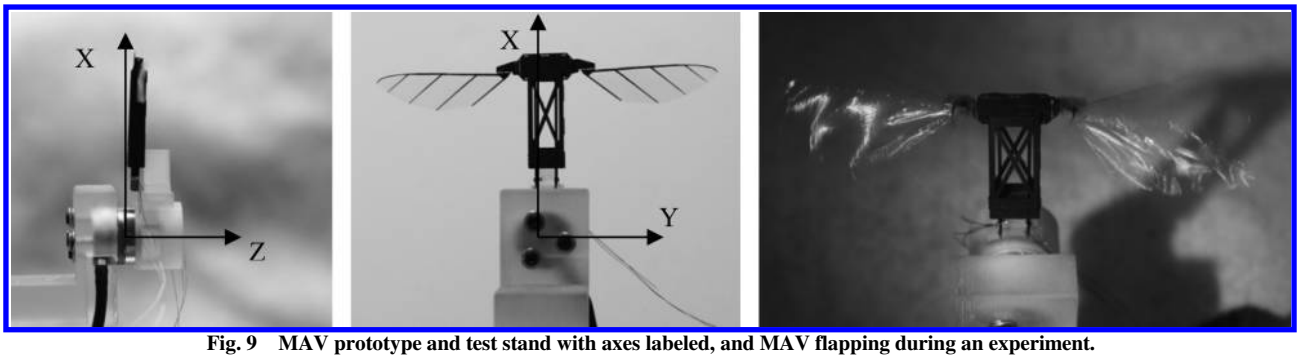

Fig. 9 MAV prototype and test stand with axes labeled, and MAV flapping during an experiment.

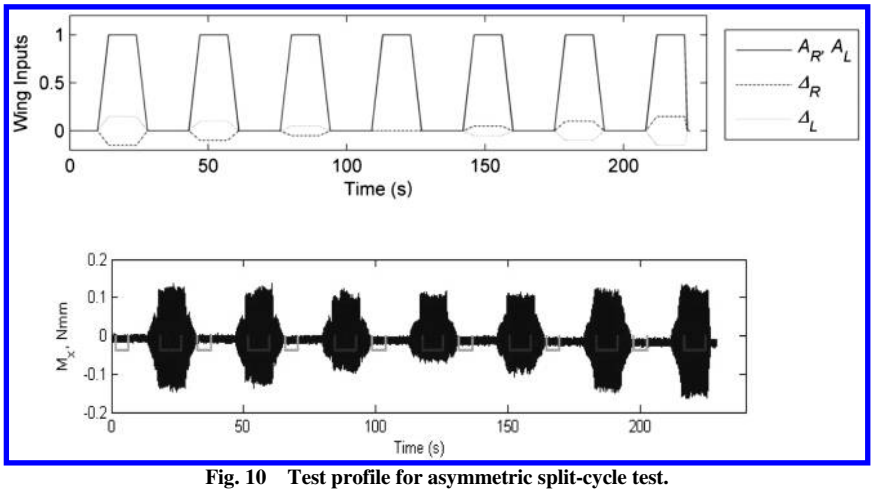

Fig. 10 Test profile for asymmetric split-cycle test.

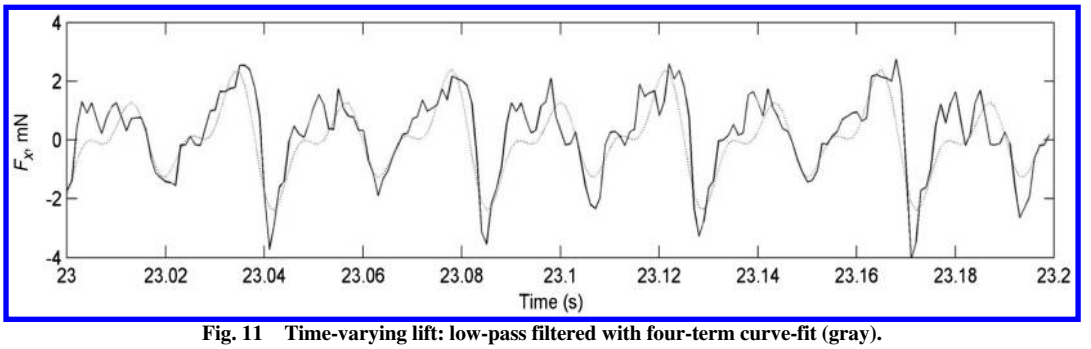

Fig. 11 Time-varying lift: low-pass filtered with four-term curve-fit (gray).

and so, for a flapping frequency of 30 Hz, 240 cycles would be averaged to create a single data point. A quiescent flow environment was created by encasing the test apparatus in a Plexiglas® enclosure ($0.6 \times 0.6 \times 0.6$ m).

The blade-element-based predictions of cycle-averaged control forces and moments are plotted versus each control parameter as dashed lines in Figs. 12 and 13. Previous work has suggested that the cycle-averaged forces and moments are most critical in determining the motion of an insect-sized flapping vehicle because higher-frequency inputs are naturally filtered by the vehicle dynamics [18–20]. The slope of each curve at the origin represents the control derivative linearized about hover and matches the control effectiveness matrix given in Eq. (21). The MAV geometric properties used in the blade element calculations are given in Table 2.

Plotted on top of these blade-element predictions are the experimentally measured values, cycle-averaged as described earlier (forces are in units of mN, moments are in mN · mm). For each abscissa value, 5 to 12 ordinate values are plotted to give an indication of the repeatability of the measurement. Take note that the mounting configuration of the MAV (shown in Fig. 9) increases the sensitivities of M_y and M_z, and the data were not adjusted to compensate for this.

For the symmetric amplitude experiment (left column of Fig. 12), the predicted relationship between amplitude modulation and F_x is clearly demonstrated, with little coupling between the other DOFs. There is some coupling with M_z. This is likely a result of a slight asymmetry between the two wing amplitudes, which generates a net side force due to spanwise flow. This side force is then greatly amplified by the aforementioned cantilevered mounting arrangement. Such an asymmetry would be easily corrected by closed-loop feedback in a final MAV design.

Asymmetric amplitude modulation is shown in the left column of Fig. 13, which plots the measured values against the amplitude of the right wing and so, at a given data point, the left wing would be complimentary. For example, when the right wing has an amplitude of 1.15, the left has an amplitude of 0.85 (these values represent 115 and 85% of the nominal amplitude A_o respectively). The predicted trend of a strong relationship between asymmetric amplitude and M_z is clearly demonstrated, with only weak coupling between the other DOFs. Furthermore, the total lift F_x remains relatively constant, indicating that the vehicle would be capable of yawing into a turn without losing lift.

In addition to amplitude modulation, the MAV's response to frequency modulation was also tested, which has been proposed as an alternative to amplitude modulation [7,8]. The results of this experiment are given in Fig. 14. As expected, the MAV generates more lift as frequency increases, but starts to saturate as the frequency departs too far from the system resonance. This suggests that

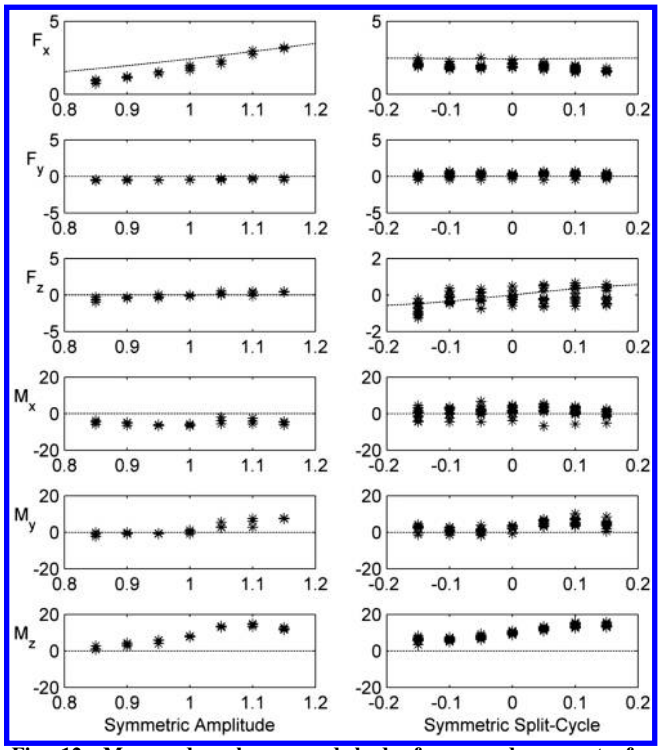

Fig. 12 Measured cycle-averaged body forces and moments for symmetric wing flapping.

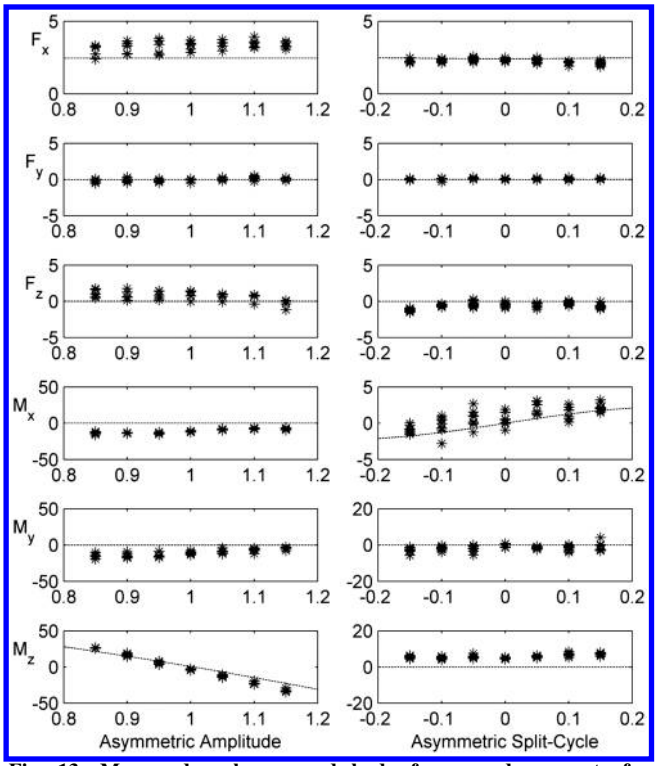

Fig. 13 Measured cycle-averaged body forces and moments for asymmetric wing flapping.

Table 2 MAV parameters used for blade-element calculations

Parameter	ω	A_0	ρ	C_L	C_D	I_A	α	w	Δx	x_{CP}	y_{CP}
Units	Hz	rad	kg · m^3	-	-	m^4	deg	m	m	m	m
Value	28	0.785	1.2	1.2	1.0	1.76e^{-7}	45	0.01	0.0005	0.001	0.03

symmetric frequency modulation may be viable as long as the range of frequencies is limited. There may yet be complications with implementing asymmetric frequency modulation because there will likely be cross-talk between the two wing flapping systems.

The split-cycle experiments, shown in the right columns of Figs. 12 and 13, are less definitive. In general, the split-cycle waveform modulation produced net forces that are useful for vehicle control, but they are less consistent and slightly lower than predicted. In the right column of Fig. 12, the predicted relationship between split-cycle modulation and F_z is somewhat weak. The upper half of Fig. 15 shows a detail view of this relationship for all 12 data sets that were obtained. The desired trend exists, but has significant variability. It should be noted that these values are very close to the noise floor of the sensor, and may be suffering from measurement noise. As long as the trend given by the data is a reflection of the actual flow physics, then it should be possible to implement closed-loop control on the final vehicle. The low magnitude of the force will only limit the vehicle's performance along that DOF. The analysis predicted no coupling between split-cycle modulation and the other DOFs, and the experiments revealed only a weak coupling, which will greatly simplify implementation of the control system. Once again, it is shown that force production remains relatively constant during split-cycle modulation, which is essential to maintain stable flight.

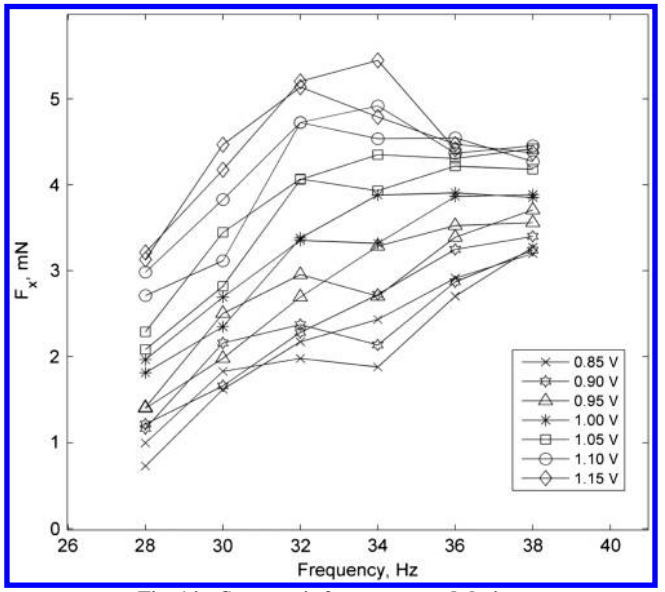

Fig. 14 Symmetric frequency modulation.

The relationship between asymmetric split cycle and M_x given in the right column of Fig. 13 is similar. The measurements match the predicted trend, but only in a stochastic sense because there is significant variability. A detailed view is given in the bottom of Fig. 15, which clearly shows the predicted trend, although there is variability.

As a whole, these force and moment measurements verify that the proposed biharmonic amplitude and bias modulation technique for flapping wing control along with discrete harmonic plant compensation does produce forces and moments in four of the five DOFs that it was predicted to affect. This is a very encouraging result and a necessary intermediate step on the way to full state closed-loop control. The fifth DOF that was not tested on the force transducer is bias modulation, which is predicted to affect the pitching moment

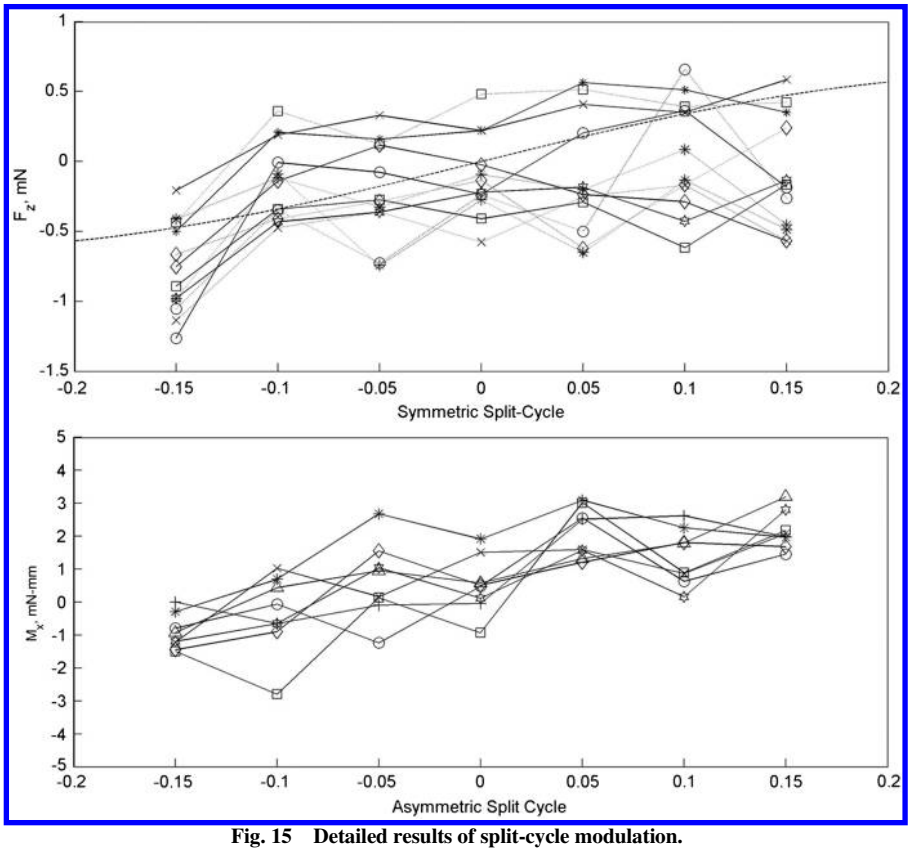

Fig. 15 Detailed results of split-cycle modulation.

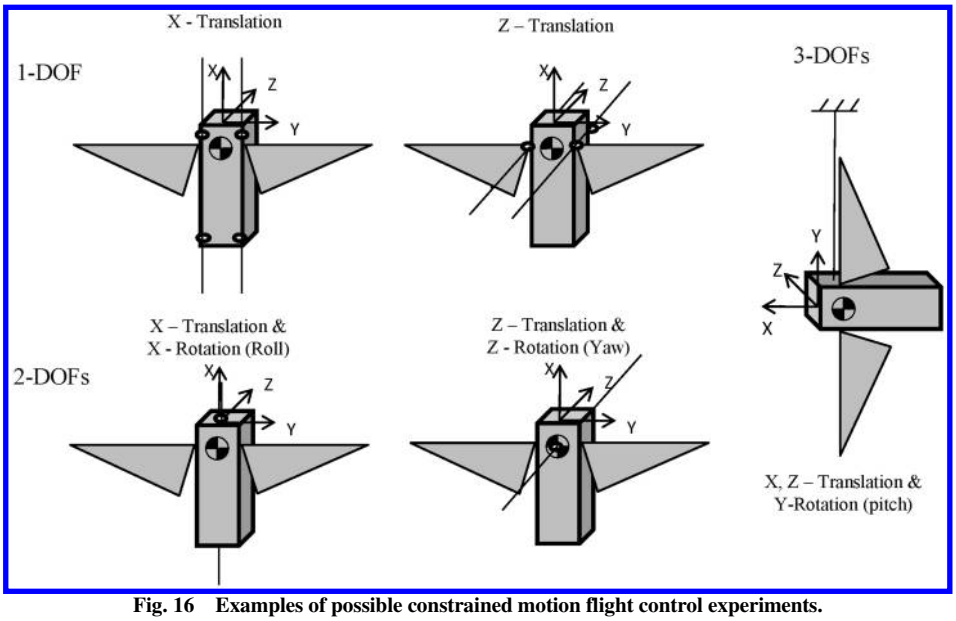

Fig. 16 Examples of possible constrained motion flight control experiments.

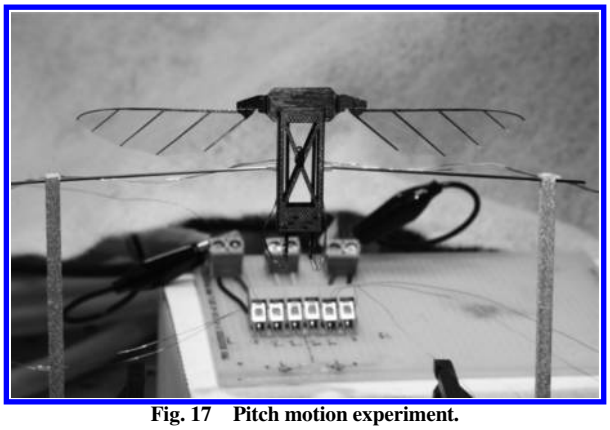

Fig. 17 Pitch motion experiment.

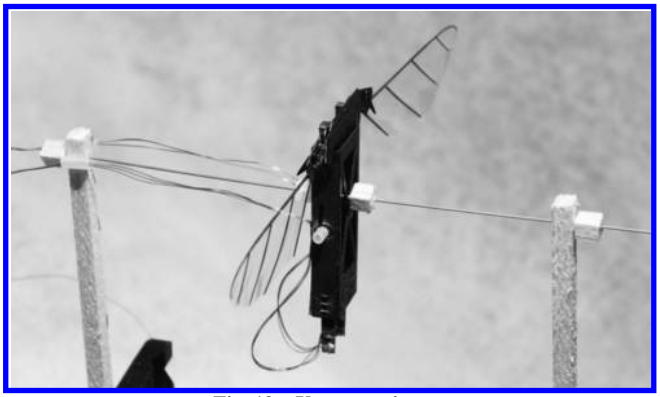

Fig. 19 Yaw experiment.

M_y. This DOF was not tested because the balance was not expected to be sensitive enough to detect the small changes in pitching moment that were predicted by the blade-element model.

An alternative approach was to use the MAV itself as the sensor by allowing it to move in a constrained environment, with certain DOFs constrained and others unconstrained. Numerous kinematic constraints can be implemented that create constrained motion environments to test one, two, or three DOFs at a time. Examples of some of the possible constraint combinations are given in Fig. 16.

For this work, two such constrained motion experiments were performed testing pitch (Y rotation) and yaw (Z rotation). The pitch experiment setup is shown in Fig. 17 where the MAV fuselage is pinned so that it can rotate about the pinned axis. Power to the actuators is supplied from off the vehicle, and so the wires will further constrain the vehicle motion. Therefore, care was taken to reduce this influence by aligning the wires with the axis of rotation so that the wires did not need to translate, but only rotate. Nevertheless, the wires inhibited the vehicle motion significantly, making efforts to quantify the resulting motion futile. Instead, only a qualitative assessment was made. The vehicle performed as expected, pitching forward and back as a result of the additional bias. Figure 18 shows video capture of this experiment in which the MAV can be clearly seen pitching forward as a result of a DC bias [η in Eq. (1)] being applied to the wing trajectory.

A second experiment tested the predicted yaw motion (rotation about the Z axis). The setup is shown in Fig. 19 in which the MAV is threaded on a steel wire so that it can rotate. Again, the actuator drive wires are routed along the axis of rotation to reduce their influence on the experiment. The vehicle was very responsive to the asymmetric flapping amplitude modulation, increasing the angular displacement in proportion to the modulated wing amplitudes, and able to yaw to

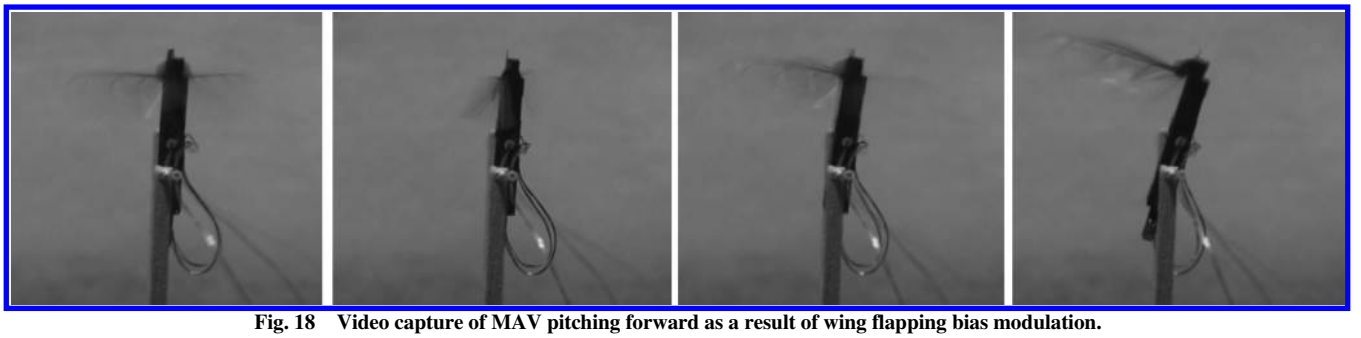

Fig. 18 Video capture of MAV pitching forward as a result of wing flapping bias modulation.

Fig. 20 MAV yawing as a result of asymmetric wing flapping amplitude modulation.

the left and right. A video capture of the resulting experiment is given in Fig. 20.

These two constrained motion experiments demonstrate the feasibility of such methods for qualitatively evaluating a proposed control technique. In the near future, efforts will be undertaken to close the loop on these DOFs. Further, additional DOFs will be tested, including *X* translation, *X* rotation (roll), and *Z* translation. If these single DOF isolation experiments are successful, multi-DOF experiments will be attempted, such as those shown in Fig. 16. These experiments will be the "training wheels" that help us learn to control flapping wing MAVs.

V. Conclusions

A novel technique, BABM, has been proposed for controlling an MAV with its flapping wings. A quasi-steady blade-element analysis of this technique predicted that it would be able to produce nearly uncoupled forces and moments on the vehicle in five DOF. To verify this analysis, over 400 flapping experiments totaling over 90 min of simulated flight time were conducted on a six-component load cell. A novel open-loop wing trajectory controller called Discrete Harmonic Plant Compensation was implemented and shown to produce the desired nonharmonic wing trajectories without the need for wing position sensors. The forces and moments measured during the experiments that followed match those predicted by the analysis and demonstrate that the BABM technique is feasible for flapping wing control of an MAV. Finally, tethered motion experiments were performed, further demonstrating the efficacy of the technique. These experiments represent the first comprehensive evaluation of a flapping wing control technique, and the most thorough to date, and pave the way for more autonomous flight testing.

For truly autonomous flight of an insect-sized MAV to be possible, further developments are required in micronavigation and attitude sensors, microcomputing, and power. In the interim, much work remains in developing flight control techniques. To continue the evaluation of the BABM technique proposed here, more tethered motion experiments will be performed in the near future, and closed-loop control of specific DOF will be demonstrated. In addition, further improvements must be made to the prototypes, which is always an ongoing effort. In particular, a vehicle capable of lifting its own weight is needed so that more vehicle DOF can be unconstrained. The current prototype has ample room for improvement, and planned refinements include optimizing the passive wing rotation joints, improving predictions of actuator performance, and optimizing the fuselage structure for weight reduction. Eventually, a tether-free experiment may be possible in which power and control commands are provided to the vehicle through a flexible tether while the vehicle is otherwise unconstrained and able to fly freely in a confined space.

Acknowledgments

This work was funded by the U.S. Air Force Research Laboratory (AFRL), Air Vehicles Directorate, under the direction of Greg Parker. We also thank Dave Doman, also of AFRL, for his enthusiastic encouragement and advice.

References

[1] Wood, R. J., "The First Takeoff of a Biologically Inspired At-Scale Robotic Insect," *IEEE Transaction on Robotics*, Vol. 24, No. 2, April 2008, pp. 341–347.
doi:10.1109/TRO.2008.916997

[2] Wood, R. J., "Design, Fabrication and Analysis of a 3DOF, 3 cm Flapping Wing MAV," *Proceedings of the 2007 Institute of Electrical and Electronics Engineers/Robotics Society of Japan International Conference on Intelligent Robots and Systems*, IEEE, New York, Nov. 2007, pp. 1576–1581.

[3] Anderson, M. L., and Cobb, R. G., "Frequency Response of a Micro Air Vehicle Wing Flapping Actuator to Non-Harmonic Forcing," AIAA Paper 2010-2708, April 2010.

[4] Anderson, M. L., and Cobb, R. G., "Techniques for Non-Harmonic Wing Flapping for the Control of Micro Air Vehicles," AIAA Paper 2010-7555, Aug. 2010.

[5] Deng, X., Schenato, L., Wu, W. C., and Sastry, S. S., "Flapping Flight for Biomimetic Robotic Insects Part I: System Modeling," *IEEE Transactions on Robotics*, Vol. 22, No. 4, Aug. 2006, pp. 776–788.

[6] Deng, X., Schenato, L., and Sastry, S. S., "Flapping Flight for Biomimetic Robotic Insects Part II: Flight Control Design," *IEEE Transactions on Robotics*, Vol. 22, No. 4, Aug. 2006, pp. 789–803.

[7] Doman, D. B., and Oppenheimer, M. W., "Dynamics and Control of a Minimally Actuated Biomimetic Vehicle Part I: Aerodynamic Model," AIAA Paper 2009-6160, Aug. 2009.

[8] Doman, D. B., Oppenheimer, M. W., and Sigthorsson, D. O., "Dynamics and Control of a Minimally Actuated Biomimetic Vehicle Part II: Control," AIAA Paper 2009-6161, Aug. 2009.

[9] Oppenheimer, M. W., Doman, D. B., and Sigthorsson, D. O., "Dynamics and Control of a Biomimetic Vehicle Using Biased Wingbeat Forcing Functions Part I: Aerodynamic Model," AIAA Paper 2010-1023, Jan. 2010.

[10] Doman, D. B., Oppenheimer, M. W., and Sigthorsson, D. O., "Dynamics and Control of a Biomimetic Vehicle Using Biased Wingbeat Forcing Functions Part II: Controller," AIAA Paper 2010-1024, Jan. 2010.

[11] Doman, D. B., Oppenheimer, M. W., and Sigthorsson, D. O., "Wingbeat Shape Modulation for Flapping-Wing Micro-Air-Vehicle Control During Hover," *Journal of Guidance, Control, and Dynamics*, Vol. 33, No. 3, 2010, pp. 724–739.
doi: 10.2514/1.47146

[12] Finio, B. M., Shang, J. K., and Wood, R. J., "Body Torque Modulation for a Microrobotic Fly," *Proceedings of the 2009 Institute of Electrical and Electronics Engineers International Conference on Robotics and Automation*, IEEE, New York, May 2009, pp. 3449–3456.

[13] Finio, B. M., Eum, B., Oland, M., and Wood, R. J., "Asymmetric Flapping for a Robotic Fly Using a Hybrid Power-Control Actuator," *The 2009 Institute of Electrical and Electronics Engineers /Robotics Society of Japan International Conference on Intelligent Robots and Systems*, IEEE, New York, Oct. 2009, pp. 2755–2762.

[14] Dickson, W. B., Straw, A. D., and Dickinson, M. H., "Integrative Model of Drosophila Flight," *AIAA Journal*, Vol. 46, No. 9, 2008, pp. 2150–2164.
doi: 10.2514/1.29862

[15] Anderson, M. L., and Cobb, R. G., "Towards Flapping Wing Control of Micro Air Vehicles," *Journal of Guidance, Control, and Dynamics*, Vol. 35, No. 1, 2012, pp. 296–308.
doi:10.2514/1.51170

[16] Anderson, M. L., and Cobb, R. G., "Evaluation of Bi-Harmonic Amplitude and Bias Modulation for Flapping Wing MAV Control," *Proceedings of the 49th AIAA Aerospace Sciences Meeting*, AIAA Paper 2011-1161, Orlando, FL, 2011.

[17] Anderson, M. L., Sladek, N. G., and Cobb, R. G., "Design, Fabrication, and Testing of an Insect-Sized MAV Wing Flapping Mechanism," *Proceedings of the 49th AIAA Aerospace Sciences Meeting*, AIAA Paper 2011-549, Orlando, FL, 2011.

[18] Fry, S. N., Syaman, R., and Dickinson, M. H., "The Aerodynamics of Free-Flight Maneuvers in Drosophila," *Science*, Vol. 300, No. 5618, April 2003, pp. 495–498. doi:10.1126/science.1081944

[19] Taylor, G. K., and Thomas, A. L. R., "Dynamic Flight Stability in the Desert Locust Schistocerca Gregaria," *Journal of Experimental Biology*, Vol. 206, No. 16, 2003, pp. 2803–2829. doi:10.1242/jeb.00501

[20] Wang, H., Ando, N., and Kanzaki, R., "Active Control of Free Flight Manoeuvres in a Hawkmoth, Agrius Convolvuli," *Journal of Experimental Biology*, Vol. 211, No. 3, 2008, pp. 423–432. doi:10.1242/jeb.011791

This article has been cited by:

1. J V Caetano, M Percin, B W van Oudheusden, B Remes, C de Wagter, G C H E de Croon, C C de Visser. 2015. Error analysis and assessment of unsteady forces acting on a flapping wing micro air vehicle: free flight versus wind-tunnel experimental methods. *Bioinspiration & Biomimetics* **10**, 056004. [CrossRef]